Publications of the Astronomical Society of the Pacific
107: 251–264, 1995 March

The High-Resolution Cross-Dispersed Echelle White-Pupil Spectrometer of the McDonald Observatory 2.7-m Telescope

ROBERT G. TULL, PHILLIP J. MACQUEEN, CHRISTOPHER SNEDEN, AND DAVID L. LAMBERT

McDonald Observatory and Department of Astronomy, University of Texas, Austin, Texas 78712
Electronic mail: rgt@astro.as.utexas.edu, pjm@wairau.as.utexas.edu, chris@verdi.as.utexas.edu, dll@astro.as.utexas.edu

Received 1994 October 20; accepted 1994 December 9

ABSTRACT. A new high-resolution cross-dispersed echelle spectrometer has been installed at the coudé focus of the McDonald Observatory 2.7-m telescope. Its primary goal was simultaneously to gather spectra over as much of the spectral range 3400 Å to 1 μm as practical, at a resolution $R \equiv \lambda/\Delta\lambda \simeq 60{,}000$ with signal-to-noise ratio of ~100 for stars down to magnitude 11, using 1-h exposures. In the instrument as built, two exposures are all that are needed to cover the full range. Featuring a white-pupil design, fused silica prism cross disperser, and folded Schmidt camera with a Tektronix 2048×2048 CCD used at either of two foci, it has been in regularly scheduled operation since 1992 April. Design details and performance are described.

1. INTRODUCTION

With the promise of availability of very large-format scientific-grade CCDs, astronomers at The University of Texas began in 1986 to consider research uses. An obvious application is high-resolution wide-bandpass astronomical spectrometry. It should be possible to display nearly the entire spectral bandpass from the UV atmospheric cutoff to the CCD near-infrared limit in a cross-dispersed echelle format fitting the Tektronix 2048×2048 CCD at spectral resolving powers of order $R = 60{,}000$, with enough space between spectra for unambiguous determination of the background. Alternatively, multiobject spectrography of 100 or more objects could be obtained with full spectral coverage at $R = 1000$ (as realized with the KPNO HYDRA multifiber positioner and bench spectrograph; Barden et al. 1993), or very-long-slit spectroscopy could be done at any resolving power, for spatially resolved spectra of extended sources.

Astronomers working at McDonald Observatory have for several decades pursued research interests in high-resolution spectroscopy. Supporting instrumentation development has continued, and we selected high-resolution, wide-bandpass spectrometry as the first McDonald Observatory application of the largest CCDs available in the foreseeable future. It quickly became apparent that the existing coudé spectrographs of the 2.7-m and 2.1-m telescopes are not readily adaptable to cross-dispersed echelle spectrometry. The 2.7-m spectrograph has been in use with a 79 gr mm^{-1} echelle blazed at 63°.5 for over 20 years, but with no simultaneous utilization of multiple spectral orders; single orders were isolated by interference filters or a pre-slit monochromator and the spectrum was scanned by a photon-counting photomultiplier (Tull 1972) or detected with Reticon linear photodiode arrays, intensified (Tull et al. 1975) and nonintensified (Tull et al. 1978), and more recently by CCDs. A very high-dispersion mode of that spectrograph uses the echelle in double-pass, with the selected spectral order isolated by a cross-dispersing grating. The spectrograph was not optimized for use with the pixel geometry of solid-state detectors, leading to relatively poor limiting-magnitude performance—a situation which was tolerated in the early years in comparison to the much poorer speed of photographic or scanner spectrometry. With a single 1872-element Reticon linear self-scanned photodiode array and the echelle, the typical high-resolution spectrum covered 15 Å at 5000 Å wavelength and the spectral resolving power could approach $R \simeq 200{,}000$ with a narrow slit (0.3 arcsec). A number of observing programs have used the echelle in double-pass and a TI 800×800 CCD at resolving power $R \simeq 500{,}000$ (Lambert et al. 1990; Hobbs and Welty 1991; Crane et al. 1994).

An interim plan adopted to broaden the passband and fill our needs until large-area CCDs became reliably available was the NSF-supported OCTICON (Oct′-i-con: [Gk okt-eight; eikon, image]). In that instrument, installed in 1984, the 1-m diameter spherical mirror of a photographic Schmidt camera of focal length $f = 1.8$ m was used to image the spectrum onto a linear array of eight 1872-element linear Reticon diode arrays arranged end to end. OCTICON was used with low-order conventional gratings, typically at $R \simeq 40{,}000$, covering typically 1600 Å of spectrum requiring two exposures to fill the gaps between arrays (see, e.g., Gies and Kullavanijaya 1987). With the successful development of large-format Tektronix CCDs, OCTICON was retired in 1989 and has been replaced by the new spectrometer ("2dcoudé") herein described.

2. SCIENTIFIC MOTIVATION

We illustrate the desired parameters for a new spectrometer by examining an example of past use of the 2.7-m coudé spectrograph. Cottrell and Sneden (1986) published a study of the CNO abundances in about 30 old disk giants. They observed features of the C_2 Swan Bands (λ~5100 Å), the CN Red System (λ~8000 Å), the [O I] lines (λ~6300 Å), and selected atomic lines in a couple of other wavelength regions. The spectral resolution employed in their study was usually $R \simeq 30{,}000$. With the large range in desired wavelengths, at least four observations were required for each star, using a 1200 gr mm^{-1} grating in first order and the 1872-element Reticon linear photodiode array detector. Since old

disk giants have relatively weak absorption features, the spectral resolution was just adequate for most abundances in their study, but proved inadequate for the derivation of reliable carbon isotopic ratios (Shetrone et al. 1993). Their study absorbed weeks of telescope time; it could benefit from higher-spectral resolution (R=60,000) and it could be completed in a few nights at most with an efficient spectrograph capable of covering the full range of their study in one or two exposures per star.

The requirements for the spectrometer were thus threefold: (a) spectral resolution sufficient to resolve blends in stellar features; (b) complete spectral coverage in the wavelength range 3400 Å to 1 μm; and (c) significantly fainter limiting magnitudes, beyond the limits of the then-existing spectrograph.

The limiting magnitude requirement immediately constrained the possible spectrographs to designs using echelles, due to their high angular dispersion which permits the spectrograph entrance slit to be large, admitting a large fraction of the flux in the stellar image under normal seeing conditions.

The resolution requirement arose from consideration of intrinsic profile widths of stellar absorption features. The narrowest stellar features occur in the spectra of cool, slowly rotating stars. For example, if $T\sim4000$ K and microturbulent velocity $v_{\rm turb}\sim1.5$ km s^{-1}, the Gaussian Doppler FWHM linewidth is $\lambda/\Delta\lambda\sim100{,}000$. Hotter, more turbulent, or more rapidly rotating stars will have broader line profiles, but if a spectrograph produces an effective resolution of about 100,000, essentially all resolvable complex or blended features will be resolved in stellar spectra.

The spectral coverage requirement involved fitting the free spectral range of each echelle order on the CCD chip. For a Littrow spectrograph, the *length* (FWHM) of a spectral order is equal (to a good approximation) to the *free spectral range* between orders, and we will frequently use these terms interchangeably. Since the physical lengths of spectral orders grow linearly with wavelength, the lengths of the reddest orders set the boundary conditions. At 9000 Å for example, the free spectral ranges for commonly available echelle gratings are about 140 Å for a 31 groove mm^{-1} R2 echelle and about 360 Å for a 79 groove mm^{-1} echelle. A requirement for acquisition of complete orders for all wavelengths up to 9000 Å on a CCD with 2048×2048 pixels forces a maximum possible resolution $R\simeq65{,}000$ for the 31 groove mm^{-1} echelle case, and much decreased resolution for the other available gratings. There are arguments not favoring selection of the 31 groove mm^{-1} echelle, forcing a compromise in the spectral coverage requirement (Sec. 4.4).

3. TECHNOLOGICAL MOTIVATION

Despite its low detective quantum efficiency (<4%) the photographic emulsion retains an enviable capability for archival storage of a vast quantity of data, and the images are readily visible to the eye. These advantages have been (perhaps temporarily) lost in the move to photoelectric spectrometry. Three major technological advances of the past two decades have now opened the door for regaining, for photoelectric spectroGRAPHY, those temporarily lost advantages previously enjoyed by the photographic spectrograph, and—far more important—have made it practical to do photoelectric spectroMETRY (formerly reserved for single-channel spectrum scanning) with a wide-bandpass spectroGRAPH. Wide-spread use of the term "spectrometer" has now largely replaced "spectrograph" in modern astronomical usage. The three major advances are:

(1) Rapid improvements in computational speed and memory capacity per dollar in workstation-class computers used for CCD control and readout.

(2) Large-area CCDs capable of detecting, at high DQE, faint images containing up to 16 million pixels.

(3) Diffraction grating technology.

Harrison (1949) pointed out the throughput efficiency and resolving power to be had with a large-area grating ruled at large blaze angles. At MIT he developed the methods for ruling such "echelles." By 1972 echelles with ruled area up to 204×408 mm and blazed at arctan 2 (63°.4, referred to as "R2 echelles"), ruled on his machine at Bausch & Lomb (now Milton Roy), became available. Echelle replicas blazed at arctan 2.8 (70°.5, R2.8) with ruled area 306×408 mm and smaller ones with blaze up to arctan 4 (76°, R4) are now commercially available.

The echelle grating's dispersive properties are a far better match to the square format of a CCD than to a linear detector array. In high spectral orders the free spectral range, FSR=λ_b/m, is a small fraction of the blaze wavelength and, as a result, light at all wavelengths is heavily contaminated by overlapping spectral orders, which must somehow be gotten rid of or—better—separately detected. That can be accomplished with cross dispersion, using a grating or prism, and a two-dimensional image detector.

4. OPTICAL DESIGN

4.1 General Considerations

Based on astrophysical requirements (Sec. 2), a resolving power goal of R=60,000—the resolution equivalent of 5 km s^{-1} radial velocity—was established. We set a goal of one arcsecond minimum slit width at the target resolving power, for high slit throughput in the presence of average seeing. Application of the grating and throughput equations (Schroeder 1987) showed these goals could be reached with an R2 echelle with a 204×408 mm ruled area, available from the Milton Roy Co, illuminated by a 190-mm diameter beam. For a detector we selected the Tektronix 2048×2048 CCD with 24-μm pixels. We selected the 2.7-m telescope for its aperture and stability and for its accessibility to adequate space for instrumentation (the large coudé room and Cassegrain instrumentation load capacity). The basic parameters of the spectrometer (beam size, camera effective focal length) were thus established. Only the design details associated with cross dispersion, high efficiency, and imaging quality in the absence of scattered and stray light remained to be worked out.

Optical evaluation of the two R2 echelles (Grating E1, the 79 gr mm^{-1} grating already in use at the 2.7-m coudé, and Grating E2, a 52.67 gr mm^{-1} echelle obtained from Milton

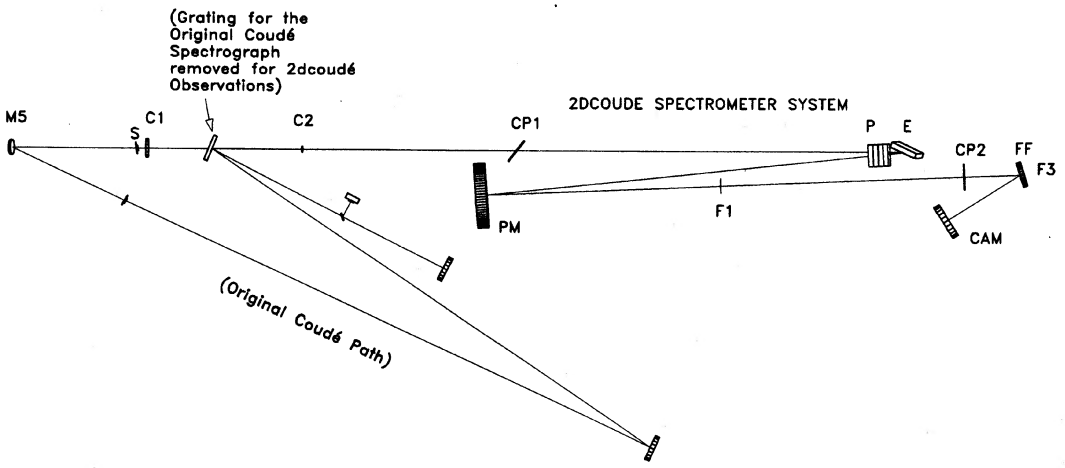

FIG. 1—The 2dcoudé optical system. S: field mirror and slit. C1 and C2: collimator primary and secondary mirrors. CP1 and CP2: aspheric corrector plates. P: Prisms. E: Echelle, PM: Pupil mirror. F1: $R=250{,}000$ focus. F3: $R=60{,}000$ focus. FF: Camera folding flat. CAM: Camera primary mirror. A field-flattening lens at F3 is not shown.

Roy early in the project showed the effective blaze angle of E1 is 63°.900 and that of E2 is 65°.293, both significantly greater than the nominal arctan 2. These updated values, combined with the parameters given in the previous paragraph, established an effective camera focal length of 775 mm for which the pixel-limited resolving power at the Tektronix CCD is 59,500 for Grating E1 and 63,000 for Grating E2.

The large, 190-mm beam size and 204×408-mm echelle dimensions ruled out use of the Cassegrain focus due to the heavy loads to be carried. The remaining options were coudé and fiber-fed fixed spectrograph. The 2.7-m telescope is equipped with a very large horizontal coudé room and spectrograph support frame in a stable thermal environment (Tull 1969), and we chose this space for the spectrometer. We aligned the spectrometer with the coudé feed, so that we could leave the fiber feed for future development, allowing us to put our full effort and resources into an efficient, high-performance optical design. These decisions have paid off in the final result, a design totally free of obscuration losses and with well-controlled optical aberrations over the 3°.7 square field of the $f/4.1$ folded Schmidt camera. The only source of vignetting, that of edge rays due to overfilling of the echelle, is fully compensated by an increased slit width enabled by the resulting higher spectral resolution (Tull 1972; Schroeder 1987).

4.2 Basic Optical Design: A Modified White Pupil Spectrograph

We used a three-tiered attack on the optical design of 2dcoudé. After an initial layout on paper in which all the preliminary decisions were reached (with the exception of the form of the camera) there remained the optimization and design confirmation steps. The GENII-PC optical design software[1] was used to optimize the design. John Lacy made available his program RAYTRACK, a powerful raytracing program. One of us (MacQueen) modified and expanded RAYTRACK to handle up to 100 surfaces and nearly unlimited numbers of rays (several tens of thousands of rays can be traced, particularly useful for covering a surface with a random pattern of rays). We used RAYTRACK for two general purposes: (1) for a preliminary look at the expected range of performance for optical concepts, and (2) for confirmation of the GENII optimization. RAYTRACK in its present form is capable of accepting the full optical system, including the telescope and spectrograph, and producing image-spot diagrams, beam-cross sections, and most other conventional optical diagnostics. It has proved to be a valuable tool in analyzing vignetting and obstructions and in testing beam clearances and overall optical performance. The current version, however, works with only a single preselected wavelength for each run and has no optimization capabilities. It handles diffraction gratings with no error that we have discovered but only in the preselected spectral order.

In Fig. 1 we show a schematic optical layout of 2dcoudé. Our design is based on a variation of the "white-pupil" spectrograph of Baranne (1972). In the white-pupil concept the system pupil at the dispersive element is re-imaged on the entrance aperture of the camera. This pupil image is fixed in position, independent of wavelength (hence the term "white pupil"). Coma is eliminated. The secondary shadow of the telescope is imaged on or near the central obstruction of the camera, eliminating losses due to variable obscuration across the field. A discussion of the improved performance due to this geometry has been given by Tull and MacQueen (1988).

Baranne's original white pupil spectrograph concept used a collimator lens in double pass. The spectrum was imaged at large scale on a spherical *miroir collectrice* which re-images the grating onto the entrance pupil of the camera. As a result, the camera is used at its greatest advantage for best control

[1]Genesee Optical Software, Inc., 3136 Winton Rd. South, Rochester, NY 14623.

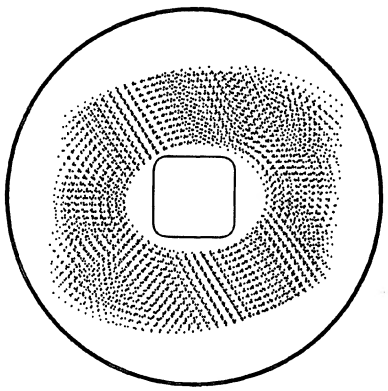

FIG. 2—Distribution of flux in the white pupil at the folding flat of the Schmidt camera. The raytraced beam cross section is shown superimposed on the mirror surface. The superimposed pupils shown correspond to rays focused at the center of the field and at the corners of the CCD for the reddest and bluest spectral orders centered near $\lambda=1$ μm and $\lambda=3400$ Å. The square represents the central hole in the fold flat. Vignetting of the pupil images due to overfilling the echelle is compensated by an increased slit width (see text).

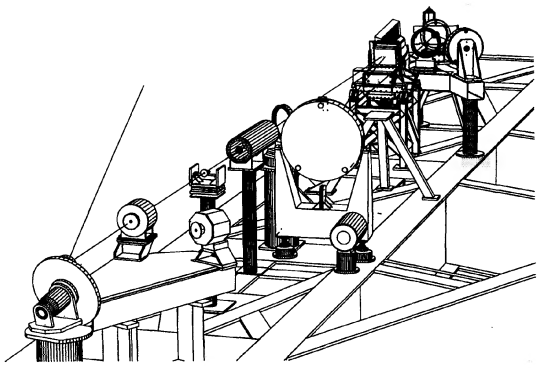

FIG. 3—Perspective view, spectrometer and frame. Not shown are the wall separating coudé and slit rooms and the pre-slit instrumentation. The slit assembly is shown for the original coudé spectrograph.

of aberrations and losses due to obscuration and vignetting. We use the more descriptive "pupil mirror" (i.e., the mirror which forms the white pupil) in place of "collector mirror." We note important differences of our design from Baranne's: we use a single-pass collimator, and the spherical pupil mirror receives dispersed, collimated light rather than a focussed spectrum. Rays are then brought to an intermediate focal surface F1, from whence they diverge to form an image of the grating on the entrance aperture of the finite conjugates camera. Two corrector plates are used: an axisymmetric asphere to correct spherical aberration of the camera mirror, and an off-centered asphere in the collimated beam to correct the spherical aberration of the tilted pupil mirror. This latter corrector must undergo a tilt to compensate anamorphic magnification of the dispersed beam, the tilt being a function of grating tilt.

This design permits using the echelle very close to the true Littrow condition. The radius of curvature of the pupil mirror (6.632 m) allows the angle between incident and dispersed rays to be quite small ($\theta=3.^{\circ}0\equiv$the angle between the incident ray bundle and the normal to the groove face) maximizing the overall spectrograph throughput efficiency (Case A, Schroeder and Hilliard 1980). In the final design the white pupil was magnified $\times1.27$ by a longitudinal displacement of the pupil mirror and imaged on the folding flat of the Schmidt camera, rather than on the corrector plate, which was figured to compensate that displacement. In this arrangement the square hole through the folding flat fits entirely within the shadow of the telescope secondary in the white pupil, independent of wavelength or field position at the final focal surface, eliminating all losses due to the center hole (Fig. 2). Imaging quality is excellent over the entire field. Losses due to the pupil mirror and its off-axis Schmidt corrector will be of order 2% for $\lambda>4000$ Å when that mirror receives its overcoated silver surface, while the white-pupil design has eliminated potentially much greater vignetting and obscuration losses (MacQueen and Tull 1988; Tull and MacQueen 1988).

The completed 2dcoudé spectrometer is illustrated in perspective view in Fig. 3. 2dcoudé, like the original coudé spectrograph (Tull 1969), lies on the horizontal plane below the observing floor of the 2.7-m telescope. Light reaches the slit after reflection from the silvered flat fourth and fifth mirrors of the coudé mirror train. 2dcoudé is supported on the main center section of the original massive coudé frame. To gain full access we retired the two original photographic cameras, including that used for OCTICON. The original coudé spectrograph remains in parallel operation, with a small camera mirror recording single spectral orders on small-format CCDs.

At C1 (Fig. 1) is the Dall-Kirkham Cassegrain collimator primary mirror. C1 is mounted in the slit housing, which penetrates the wall of the coudé room. The secondary mirror C2 is mounted on a separate pedestal. CP1 is the aspheric corrector for the spherical pupil mirror PM, and P marks the two 30° cross-dispersing prisms of broadband AR-coated fused silica. The prisms are in double-pass and are mounted with the echelle grating E on a cradle which serves to tilt prisms and echelle for selection of the wavelength region to be centered on the CCD. The echelle is located at a pupil of the system.

The prisms are of Corning quality 1A fused silica, selected and supplied by Glass Fab. Inc.,[2] and were figured by Tucson Optical Research Corporation.[3] The material was selected for its high ultraviolet transparency, its homogeneity, and its excellent dispersion, giving the least variation of spacing of the spectral orders of all the glasses considered, and much less variation than can be attained with either a grating or prism cross disperser. Corning was unable to supply blanks in thicknesses greater than about 125 mm, and it was necessary to optically contact pairs of 15° wedges, each

[2]P. O. Box 1880, Rochester, NY 14603.

[3]210 S. Plumer Ave., Tucson, AZ 85719. All other optical shop work was accomplished by Don Loomis, Custom Optics, 3624 Ave. de Montezuma, Tucson, AZ 85749.

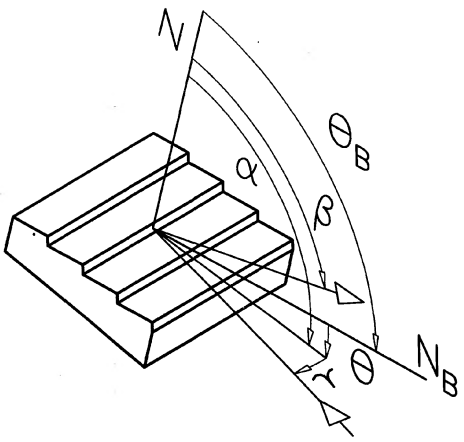

FIG. 4—Definitions of the echelle parameters; see text.

having maximum thickness 72 mm, to obtain two 30° prisms.

PM is the pupil mirror, with its center of curvature near the echelle at point CC. PM receives light dispersed horizontally by the echelle and vertically by the prisms and produces a large-scale cross-dispersed spectral format at the highest resolution focus F1. After diverging through F1 and passing through the Schmidt corrector CP2, the rays form the white pupil WP, coinciding with the folding flat FF. The final focal surface F3 is flattened by a lens in front of the dewar window. The CCD in its dewar can be mounted at F3 to obtain spectra at resolving power $R=60{,}000$ or at the very-high-resolution focus F1 (without the field flattener lens) for $R=250{,}000$ over limited spectral ranges. The designation F2 has been reserved for a possible future intermediate-resolution camera.

4.3 Choice of Echelle Geometry

We adopt the conventions used by Schroeder and Hilliard (1980) for the geometric parameters (Fig. 4):

α, β≡angles of incidence and dispersion at the echelle.

θ≡angle between incident ray and the normal to the groove face (α, β, θ are all measured in the $y-z$ plane normal to the grooves).

γ≡angle between the incident ray and the $y-z$ plane.

Alternate geometries in echelle spectrograph design are classified (Schroeder and Hilliard 1980) as Cases A, B, C in which Cases A and B have the echelle in-plane ($\gamma=0$) and Case C off-plane (γ nonzero). In Case B, $\alpha<\beta$ and groove shadowing losses are important. This is an undesirable geometry and Case B is rejected. In Case C, spectral lines are slanted at angle 4γ for an R2 echelle. Line slant is a function of wavelength if the cross-dispersing prism is in the grating's incident beam, due to the variation of γ with wavelength. The average line slant can be reduced to zero by counter-rotating the spectrograph slit.

Schroeder and Hilliard (1980) derived the effects of echelle orientation on the theoretical blaze efficiency and on the throughput of a complete echelle spectrograph. They concluded that the throughput-resolution product is equal within a few percent for Cases A and C at small θ or γ but drops off for Case A as θ increases beyond 3°. Case C, with slit counter-rotated to compensate the line slant, also falls off, closely following Case A. The best throughput-resolution product occurs for Case A with $\theta<3°$ while Case C (with slit parallel to the grating rulings) is nearly independent of γ. The overall throughput-resolution product over a spectral order favors Case A by a few percent. We adopt their conclusions and recommendations, modified by the predicted vignetting and obscuration losses for an echelle grating of finite size.

Vignetting loss due to the finite width of an overfilled grating increases with θ; thus we strive to keep this angle as small as is practical. At $\theta=6°$ the vignetting loss would be about 18% for our geometry, in addition to a 7% loss in the peak blaze efficiency (Schroeder and Hilliard 1980). There is a compensating factor: if the slit is overfilled, as frequently occurs with mediocre seeing in high-resolution slit spectroscopy, the throughput-resolution product maximizes when the beam diameter is typically 20% greater than the grating's projected length, the advantage being typically 7% (Schroeder 1987, p. 250; Tull 1972).

The design of our spectrometer is Case A with $\theta=3.^{\circ}0$ and cross-dispersing prisms in double pass. The overall throughput-resolution product is close to the maximum value possible due to the factors discussed by Schroeder and Hilliard (1980). The vignetting loss is small (7%); for average seeing conditions, this loss is compensated by the slitwidth increase.

The selection of double-pass prisms for our design took into account the advantages and disadvantages listed:

Advantages:

(1) A unique pupil can be better approximated (all the dispersing elements are optically close together).

(2) The size of the prisms is minimized.

(3) Half as many prisms are needed.

(4) The angle θ is minimized.

Disadvantage:

The echelle sees a variation of $\pm0.^{\circ}9$ in γ due to the first pass through the prisms, resulting in variable line slants up to $\pm3.^{\circ}7$. The variation of slant within one spectral order is negligibly small (about 8 arcmin with a 52 gr mm^{-1} echelle), readily corrected in data reduction, and it seemed clear that the advantages of this configuration (including the obvious economic ones) significantly outweigh its disadvantages.

4.4 Choice of the Echelle Grating

For an echelle, groove spacing affects only the width of the blaze profile and the free spectral range; these are equivalent at Littrow. In the 1988 Milton Roy catalog four rulings were offered for echelle gratings at the desired blaze angle ($63.^{\circ}5$) and size (204×408 mm); these had 31.6, 52.6, 79.0, and 316 gr mm^{-1}. Figure 5 illustrates the cross-dispersed echelle format superimposed on the Tektronix TK2048M CCD, for the 52 and 79 gr mm^{-1} gratings. The 316 gr mm^{-1} grating is not appropriate for this application. Our original 79 gr mm^{-1} echelle, when used in 2dcoudé, produces orders of width greater than the CCD for all orders to the red of 3900

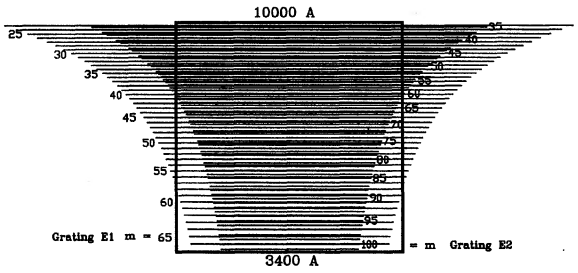

FIG. 5—Spectral image format. Each line represents the length (FWHM) of a spectral order. Formats are shown for two echelle rulings; the square represents a CCD with 2048×2048 24 μm pixels.

Å. The 31.6 gr mm^{-1} grating would produce a format completely within the boundaries of the CCD but the minimum order separation would be 6 arcsec, leaving insufficient interorder background free of contamination from starlight under normal seeing conditions with a long slit. The 52 gr mm^{-1} echelle separates orders 10 arcsec at minimum (in the IR), increasing to 20 arcsec in the UV. Spectral orders are completely contained within the CCD boundaries only for wavelengths shortward of 5600 Å; at most, two exposures are needed for full coverage in the red. The 52 gr mm^{-1} grating best fulfills the requirements of the spectrograph, while the 79 gr mm^{-1} grating will find use where greater spectrophotometric uniformity is important or to reach selected wavelengths which lie off-blaze for the 52 gr mm^{-1} grating.

4.5 Echelle/Prism Assembly

The spectrograph was designed primarily for use with a large-format Tektronix TK2048 CCD with 24 μm pixels. Some spectral orders, using the two available echelles, are longer than the width of the CCD. For this reason, and to allow use of smaller format CCDs such as the TI 800×800 with 15.24 μm pixels, it is necessary to provide a method for the observer to center any desired wavelength and spectral order on the detector; there are advantages to be able to do this to within a few pixels, in both x and y. This could be done by moving either the detector or the spectrum. If the CCD is to be moved then the camera's flat field of excellent image quality must be much larger than the CCD, an expensive option. We selected a fixed CCD, movable image option. The echelle and prisms, mounted in a system pupil, were given rotations to accomplish the required image translations. This option allows the camera to be designed with excellent imaging quality over only the area of the largest CCD planned for use.

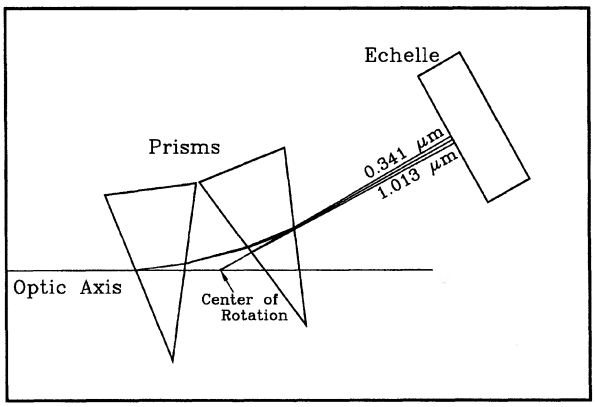

FIG. 6—Echelle/Prism configuration. The image may be shifted vertically on the CCD by rotating the entire assembly about the center of rotation labeled. See text for explanation. (Echelle shown tilted to order zero for clarity.)

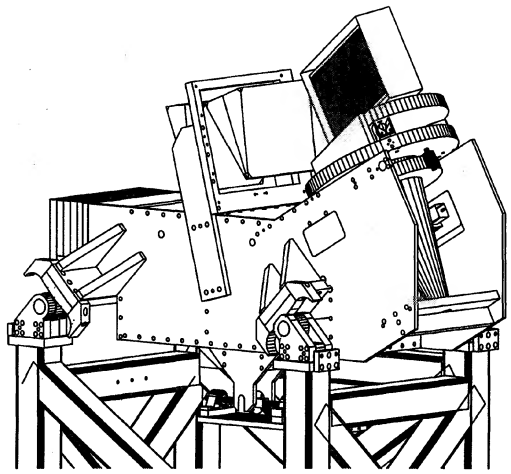

FIG. 7—Echelle/Prism cradle. Rotation of the echelle on its axle shifts wavelengths. Order selection is accomplished by rocking the cradle on its rockers, which are arcs concentric with the axis of rotation shown in Fig. 6. The prism cells are not shown, for clarity.

Figure 6 shows the echelle and prisms, with principal rays of intermediate and extreme wavelengths. The echelle and prisms are mounted in close proximity to minimize required dimensions for the prisms. Translation of the spectrum horizontally is easily accomplished by rotating the echelle (shown schematically with zero tilt) about an axis coincident with its central groove. Vertical translation is accomplished by rotating the entire assembly, prisms and echelle, about a horizontal axis intersecting the optical axis of the collimator midway between the two prisms. This rotation axis provides the minimum risk of vignetting, both at the prisms and at the echelle, as function of rotation, and it keeps angle γ zero for the central wavelength at all tilts.

A perspective view of the echelle/prism cradle assembly, generated with AutoCAD software,[4] is shown in Fig. 7. The grating is mounted on a conical shaft, the upper end of which carries a friction-drive wheel supported radially by a pair of rollers on ball bearings. One of these rollers is driven by a stepping motor providing 0.001 rotation of the echelle per motor step; the other provides the friction drive for the shaft encoder, with the same resolution. The lower end of the shaft is supported by a ball thrust bearing. A spring-loaded roller provides a restoring force against the friction-drive wheel. The entire cradle supporting the echelle, its drive system, and the prisms is rotated, rocking-horse style, on four short rockers concentric with the horizontal axis between the prisms.

[4]AutoCAD Release 11; Autodesk, Inc., 2320 Marinship Way, Sausalito, CA 94965.

One of these rockers provides friction drive of a second shaft encoder. Rotation about this axis is provided by a ball screw tangent drive and stepping motor and is resolved to 0".001. Counterweights balance the cradle and the echelle. The prisms are mounted in a fixed orientation on the cradle; at its normal tilt the prisms are at minimum deviation to minimize aberrations. As the assembly tilts on its rockers through ±2°, the prisms violate this condition, but the change of aberrations is negligible. The deviation due to the prisms remains nearly constant; translation of the spectrum vertically is accomplished by the change in tilt of the echelle.

The drive motors are controlled by the spectrograph control computer, which also reads the encoders. Once the rotations are calibrated, the observer has available a set of commands allowing him to select a wavelength and spectral order and the computer drives the assembly to center these on the CCD.

4.6 Stray Light Control

Stray light, by definition, wanders from its prescribed course. Some eventually finds its way to the detector to produce extraneous images and general background illumination. This can result from reflections not properly accounted for in the design of the system. Scattered light, on the other hand, follows the same paths through the system as do the image-forming rays but undergoes small-angle deviations due to scattering interactions at optical surfaces. Stray light is thus distinguished from scattered light, which manifests itself in the wings of the instrumental profile and, between orders, in the wings of the stellar image profile.

In this section we discuss six known sources of stray light, existing or potential. Five have been eliminated or controlled in the 2dcoudé spectrometer. The sixth was not anticipated and cannot readily be eliminated except in original design. The sources are tabulated here and discussed in turn below:

(1) Reflections from refractive surfaces.

(2) Reflections from the optically contacted prism pair interfaces.

(3) Dispersed light refocused by the collimator.

(4) Light transmitted by the slit and multiply-reflected between the mirrors of the Cassegrainian collimator.

(5) At F3, direct illumination of the CCD through the central hole in the fold flat.

(6) Narcissus: the so-called "Picket Fence."

Ideally, stray light sources should be blocked as early in the system as possible, to reduce scattering from optical surfaces.

4.6.1. Reflections from Refractive Surfaces

The spectrograph was designed such that light singly reflected from the refractive surfaces would be deflected away from the camera. All refractive surfaces have antireflection coatings averaging 1/2% reflectance per surface within the pass band 3500 to 9000 Å,[5] with no reflectance peaks exceeding 1% within the passband. In the following we consider each of the refractive elements.

[5]Continental Optical Corp., Hauppauge, NY 11788.

(a) Corrector Plate CP1: This plate is tilted to compensate for anamorphic effects on the spherical aberration correction, due to the echelle. The theoretical tilt angle is about 38% but there is no theoretical requirement on the arithmetic sign of the tilt. We tilted the plate in the direction that sends reflected light toward the west, where it will be absorbed by the coudé room walls. Light internally reflected within the corrector plate could produce halo images of point sources at the final focal plane; see (b).

(b) Corrector Plate CP2: The corrector for the folded Schmidt camera is used at normal incidence. Due to the A-R coatings a maximum of 0.01% of the total incident light at any given wavelength will be directed forward into the camera after two internal reflections; this component is uncontrollable except by the A-R coating. The size of the resulting halo can be estimated from the slope variations of the figured surface of the corrector plate. For a ray refracted by a corrector plate (figured on one side) at angle i' there is a doubly reflected ray of reduced intensity at angle i'' such that $i''-i'=2ns$ where n is the refractive index and s is the local slope on the figure surface. For CP2 the maximum slope is 0.0005 radians, producing a halo of radius 0.4 mm at the focal plane. We can estimate a mean intensity within the halo. If light from a point source (defined as a source illuminating 1 pixel in the focal plane under perfect imaging conditions) is incident on the corrector plate then 0.01% of that light will be distributed over an area of radius 0.4 mm covering 820 pixels of the TK2048 CCD. Assuming uniform illumination, the radiant flux falling on any pixel within the halo is 1.2×10^{-7} that in the primary image pixel. Even allowing for possible factors of 10 variation, this intensity will be undetectable in the presence of other sources of background radiation and noise; it is well below the observed wings in the instrumental profile (Sec. 5.1).

Griffin (1969) used a clean, high-resolution solar spectrum in the O_2 telluric A band, obtained with the McMath solar telescope and double-pass spectrograph, to determine the effects of the Arcturus Atlas (Griffin 1968) instrumental profile on deep absorption lines. He found that a convolution of the McMath solar spectrum with the Arcturus Atlas instrumental profile came within 1% of matching the observed Arcturus Atlas spectrum. In particular the flat bottom of a line at 7597.4 Å, which has central intensity near zero in the solar spectrum, has an intensity of about 4% of the nearby continuum in the Arcturus Atlas and in the convolution of the solar spectrum and the Arcturus Atlas instrumental profile. Such degradation is not observed when Gaussian absorption lines are convolved with a Gaussian instrumental profile, demonstrating that the damage is due to the non-Gaussian extended wings of the instrumental profile.

It may be possible to use this information to estimate the damage done by the halo produced by internal reflection in the corrector plates: the wings of the Arcturus Atlas profile between 0.5 and 1.0 Å from the central peak varies from 10^{-3} to $10^{-3.5}$ of the central intensity. The halo predicted for the corrector plate has a calculated mean intensity 1.2×10^{-7} the peak of a single-pixel point image in a ring of radius 0.4 mm, corresponding to 1.0 Å. The effect of this halo must be some 4 orders of magnitude less than that of the observed

wings in the instrumental profile, assumed similar to the Arcturus profile. No observable effect on central depths of absorption lines is expected.

(c) Prisms: Each of the two 30° prisms is made up of a pair of 15° wedges of fused silica, with outer surfaces A-R coated and the interfaces contacted through an index-matching fluid. These surfaces are flat. Any light reflected from a flat surface nearly normal to the incident ray is a potential source of focused ghost images at the camera focal plane. Angles of incidence for the principal ray at the central wavelength are 22°±5° at all coated prism surfaces, so that all singly reflected light is directed away from the principal ray at angles of 34° to 54°. Rays undergoing second and third reflections will have intensity less than 0.01% of the transmitted ray but these surfaces tilts defeat any tendency for rays to enter the camera. The prism edges and ground surfaces have been painted black after final assembly, and the prism cells are black anodized. Black paint has also been applied to exposed surfaces of the whiffle-tree prism supports.

4.6.2 Reflections from the Prism Pair Interfaces

The 30° prisms as originally assembled were individually mounted at minimum deviation with the 15° wedges contacted with Cargille Type 50350 silica index-matching liquid.[6] The published refractive index of the oil and the computed reflectance of the surfaces are given as functions of wavelength in Appendix A.

As first assembled, the oiled surfaces had a number of residual bubbles, which were reflective. These surfaces were normal to the incident radiation and became important sources of ghost spectral images at the 2dcoudé focal planes. In the final reassembly of the prisms a more uniform oil film was achieved, with greatly reduced residual bubble count and area. Any residual effect was eliminated by changing the tilts of the prisms ±3°, the apices of the prism pairs being tilted 3° toward each other. In this configuration the assembly remains at minimum deviation while the individual prisms do not. Raytrace analysis has indicated undetectable degradation of performance and has shown that straylight images are excluded from the camera field of view.

4.6.3 Dispersed Light Refocussed by the Collimator

With the spectrum centered on the CCD, the collimator is illuminated by the first side-lobe of the blaze profile, which can be redirected back into the spectrometer. Raytracing showed that masks can block most of this source: a peripheral mask of inside diameter 205 mm at the collimator primary, a central occulting disk of diameter equal to that of the collimator secondary mirror at the focus of the collimator primary, and two occulting disks mounted in the collimated beam 4.0 and 4.5 m from the primary are effective at blocking this flux after reflection from the collimator. Central stops supported by spider assemblies of thin piano-wire struts under tension have been mounted in the collimated beam. With masks in place, in a worst case only 2% of the sidelobe flux escapes as stray light. In the sidelobes the theoretical intensity is typically 2% of blaze maximum; the escaping stray light therefore amounts to 0.04% of blaze maximum. Of this, most diverges away from the following optical components, eventually being absorbed safely in the black-painted walls of the coudé room.

4.6.4 Multiply Reflected Light Between Collimator Mirrors

Incident rays transmitted by the entrance slit inside the shadow of the telescope secondary can be multiply reflected between primary and secondary of the Cassegrainian collimator. Raytracing does not reveal the existence of such rays, which should have been blocked by the telescope secondary. However, diffraction at the slit and scattering from the telescope optical surfaces tend to fill in the secondary shadow, giving rise to misdirected white-light ray bundles due to two and three reflections between the mirrors of the collimator, visible at the collimator secondary as rings of white light slightly larger in diameter than the secondary itself. Light due to two such reflections from each mirror converges to form an image of the slit 10.7 m from the collimator primary, very close to the echelle. This image is easily observed visually. Additional rays can be three-times reflected into a bundle of greater convergence.

Because they do converge, these rays can be blocked by occulting disks within the central shadow in the collimated beam. Partial blockage of this source occurs at the occulting disks required for Source (3); the best location for catching the residual is at the echelle, where a small occulting disk within the secondary shadow will suffice.

The secondary mirror and occulting disks have been provided with central holes that can be opened to transmit a laser pencil-beam for use in spectrometer alignment.

4.6.5 Direct Illumination of the CCD Through the Central Hole in the Fold Flat

Any light falling inside the shadow of the telescope secondary constitutes a potential source of straylight at focus F3. Unless blocked, this flux can pass through the central hole of the camera's folding flat, where some can scatter from the field-flattener lens and dewar window onto the CCD. Sources include light multiply reflected between the collimator mirrors, and any unwanted radiation in the coudé room not originating at the slit. Some of these sources are adequately blocked as discussed in the previous sections. The remainder is blocked by a straylight mask mounted in front of the central hole. This mask can be seen in Fig. 8; it was installed following tests with an occulting disk centered on the camera's corrector plate, which eliminated stray white light previously observed in the gaps between ultraviolet spectral orders.

4.6.6 Narcissus

What we describe as the "Picket Fence" straylight source is a single row of apparent emission lines, slightly defocused, nearly uniformly spaced, seen visually at both focal surfaces F1 and F3 and detected by the CCD at F3. The source of

[6]R. P. Cargille Laboratories, Inc., 55 Commerce Rd., Cedar Grove, NJ 07009; see Appendix A.

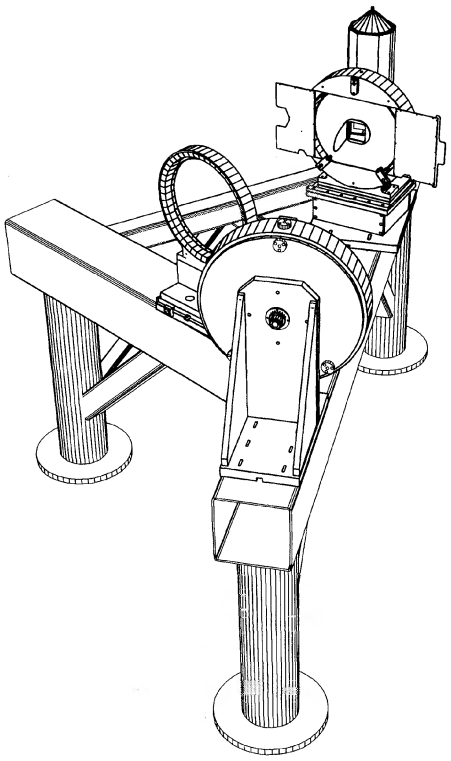

FIG. 8—The folded Schmidt camera and CCD dewar. A straylight mask is seen projecting forward from the central hole of the folding-flat mirror.

these straylight images is "narcissus," a potential problem of all optical systems with sensitive image detectors: as manifested in a spectrograph it is characterized as light reflected from the CCD back to the grating, where it undergoes a second dispersion, forming a series of images, one image for each spectral order of the primary spectrum at the detector. In 2dcoudé there are three such sequences possible corresponding to spectral orders $m-n$, where m is a spectral order falling initially on the CCD and $n=0$, 1, 2, 3. For $n=0$ light reflected from the CCD is returned by the echelle to the slit, dispersion having been cancelled. In orders $m-n$, $n\neq 0$, dispersion is reduced to $-n/m$ that in single pass. Light in orders $m-1$ to $m-3$ (for echelle E2) falls back on the camera and the CCD, the reduction of dispersion being adequate to produce images appearing to be nearly in focus, and at the same time to increase intensity to an annoying level. The wavelength band within each image is limited by the width of the reflecting area (the CCD and immediate surroundings) in the camera focal plane and the number of images is limited by the height of the reflecting area, i.e., the number of spectral orders in the image format. If the echelle is rotated each image remains nearly fixed in position but changes its color. Of the three possible sequences lying within the camera FOV only two may be detectable for any given echelle setting.

The locations and visibility of the images are functions of the echelle ruling. For echelle E1 (79 gr/mm) only sequences $n=1$ and $n=2$ fall within the camera FOV. There may be other geometries in which the effects are minimized; in particular other values of θ may yield interesting cases to investigate.

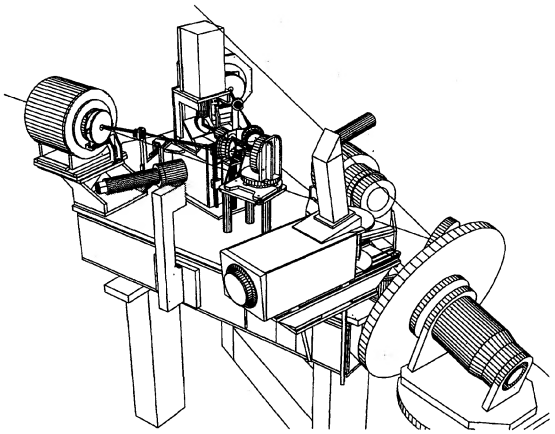

FIG. 9—Pre-slit optical bench and instrumentation. Starting from the coudé fifth mirror turret the instruments are the calibration source, image rotator, autoguider mirror, autoguider (the uppermost box houses the down-looking CCD), an eyepiece (on west edge of the bench), the slit mechanisms for both spectrographs. Autoguider zoom lenses are shown in place. When these lenses are retracted the entire 6 arcmin field covered by the field mirror is imaged by the CCD camera lens.

The prisms, too, participate in the double-pass dispersion of the light reflected from the CCD. A prism produces only a single order of dispersion. The second pass cancels the dispersion of the first, after reflection from the echelle, accounting for the single row of pickets which lies across the center of the camera field of view.

A possible solution for elimination of narcissus is a design similar to the ESO EMMI (Dekker et al. 1986) in its use with an echelle in a white pupil spectrograph. In this instrument cross dispersion is done by a dispersive element in the white pupil. A mask at the first focus could assure that stray light reflected from the CCD is blocked before reaching the echelle. A nonzero value of γ can also be used to redirect the stray light away from the camera.

4.7 Spectrometer Front End

In the original coudé spectrograph of the 2.7-m telescope the slit and collimator mirror lie along a line 25° east of north, with the grating table and photographic cameras along a north-south centerline (Tull 1969). 2dcoudé now occupies the N-S centerline (Fig. 1). We rebuilt the preslit optical bench, adapting it to serve both spectrographs (Fig. 9). Two new mirrors feeding the new 2dcoudé spectrometer were mounted on the fifth mirror turret, selectable by rotation of the turret: these receive light from the telescope and from the solar port, respectively. The solar port is a translucent diffusing window in the roof of the slit room, directly above the fifth mirror turret, from which diffuse sunlight may be fed to either spectrograph; this is frequently used to obtain solar spectra integrated over the Sun's disk, useful for planetary comparisons, spectrometer tests, etc. The old optical bench was rebuilt to support a new optical table, a 1-in.-thick steel plate filled with an array of tapped holes on a 1-in.×1-in. grid. On this table are mounted the calibration source, image

rotator, autoguider, and eyepiece, any of which may be used with either spectrograph, as well as the two slit assemblies.

For each of the two spectrographs we built a slit assembly supporting a concave spherical stainless-steel field mirror covering a field of view 6 arcmin in diameter, which directs light to the autoguider camera. Centered in the mirror is the slit plug, a 25.4-mm diameter interchangeable cylinder of stainless steel with front surface figured to the same curvature as the field mirror, and having a fixed slit cut through its center by electric discharge machining. There are 18 such slits, with widths from 83 μm to 1 mm (0.″20 to 2.″40) and lengths from 3.5 to 12.8 mm (8″ to 30″). The autoguider optical system has a two-position zoom, placing the full 6.′0 finding field or the magnified 1.′0 guide field on the autoguider CCD.

5. 2DCOUDÉ PERFORMANCE

5.1 The Instrumental Function

The instrumental profile of a spectrograph defines its resolving power, from the width of the core. The scattered-light characteristics in the direction of dispersion are manifested in the intensity distribution in the extended wings, primarily due to the properties of the grating. Griffin (1969) showed that single-pass grating spectrographs are affected by errors in the measurement of equivalent widths due to the wings of the instrumental profile. He further showed that the effects can be markedly improved by use of a double-pass scanning spectrometer with intermediate slit of width comparable to the entrance and exit slits, but at greatly reduced throughput efficiency and spectral coverage. Nevertheless, single-pass grating spectrographs have enjoyed continuing success and wide use in astronomy due to their relatively high throughput efficiency and broad spectral coverage. Continued research at Milton Roy has produced echelle gratings that are virtually free of detectable Rowland ghosts (Loewen 1993), with resultant improved performance in single pass. For the most exacting research purposes however, it is advisable to test individual gratings to determine the extent of the wings and presence of ghosts. It is important to understand the effects of the instrumental profile when interpreting equivalent width measurements. Griffin's papers have been an important contribution to that understanding. In Griffin's (1969) discussion of the effects of the instrumental profile on observed spectra, he listed the contributors to the instrumental profile of the Arcturus Atlas (Griffin 1968) as

(i) The main peak,
(ii) Rowland ghosts,
(iii) Diffracted wings,
(iv) Small-angle scattering in the optical system,
(v) Halation and scattering in the photographic emulsion,
(vi) True scattered light.

For spectra obtained with a CCD we eliminate item (v) and add as potential sources

(vii) Internal reflections and interference effects in the CCD,
(viii) Widening due to CCD transparency,
(ix) External reflections (stray light images),
(x) Charge transfer inefficiency.

Items (vii) and (viii) are the CCD analogs of photographic halation and emulsion scatter. In a CCD photons traveling through a semitransparent silicon chip release charge pairs at some depth into the silicon, some of which migrate to the potential wells forming the neighboring pixels and contribute to image spread. The degree of spread is a function of wavelength (due to the wavelength dependence of silicon transmittance), silicon thickness, and the focal ratio of the camera. Photons transmitted through the full thickness of the silicon may be reflected, contributing further to image spread and to interference fringing, leading to decreased resolving power with increasing wavelength. Item (ix) could be included in (vi) but it is useful to separate consideration of the general background scattered light from the stray light. In fact, stray light may not be detectable in the conventional test for instrumental profile, which utilizes a nominally monochromatic source and therefore fails to illuminate regions of the spectrograph which may give rise, upon reflection, to stray-light images.

To measure the instrumental profile of the 2dcoudé spectrometer, we obtained spectra of a He–Ne laser source at the F1 and F3 foci. The dispersing element was echelle E2. The data for the F3 focus will be discussed here.

The natural width (FWHM) of the 6328 Å line for the He–Ne laser is expected to be 1.7 GHz, or 0.023 Å (Bloom 1966). This agrees with the observed FWHM (0.025 Å) of the double-passed echelle instrumental profile obtained with the coudé spectrograph and scanner, using echelle E1 (Tull 1972). The line is narrow compared with the projected slit-width matched to the CCD pixels, making it an excellent test probe.

A He–Ne laser uniformly illuminated a diffuser in the calibration lamp housing. A lens in front of the diffuser produced an $f/33$ beam with virtual pupil at infinity as seen from any point over the full length of a 12.856×0.083 mm slit. At the CCD the projected slit dimensions were 0.0083 ×1.621 mm. The camera was carefully focused on the TI 800×800 CCD by minimizing the FWHM of the slit image; at the camera's $f/4$ focal ratio the sensitivity of focus settings is about 0.030 mm for a measurable change of image FWHM near focus. To obtain unit signal/noise ratio in the far wings of the profile, where the residual intensity is expected to be some 5–6 orders of magnitude below the peak intensity at line center, it was necessary to co-add many exposures short enough to avoid nonlinearity effects near pixel saturation. The maximum linear signal range for this CCD system is about 7500 ADU (A/D converter units) where 1 ADU≃6 detected photons. For S/N=1 when the signal is 10^{-6} below the peak, and accounting for the known readout noise of 15 electrons/pixel/readout, we required the summation of 110,000 1-pixel-wide spectra. To achieve this we obtained 1100 spectra each of width 100 pixels. We alternated these observations with dark exposures, which we subsequently subtracted prior to extraction of the spectra. We did not attempt to flat field the laser images, since the extraction of a spectrum spread over 100 pixels provides a first-order averaging over pixel-to-pixel CCD sensitivity variations.

Figure 10 shows the reduced spectrum on a logarithmic flux scale. To generate this spectrum, we first co-added the

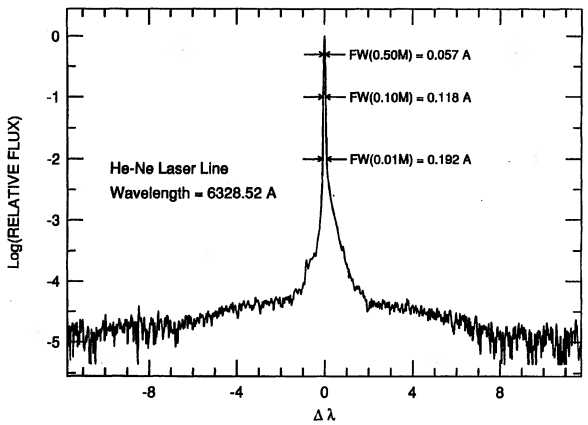

FIG. 10—The instrumental function at the $R=60{,}000$ focus, obtained from the summation of many spectra of the He–Ne laser line at 632.8 nm. Note that the flux scale is logarithmic, normalized to unit flux at the laser line peak. The full widths (FW) of the line profile at 50%, 10%, and 1% of the maximum flux have been noted in the figure.

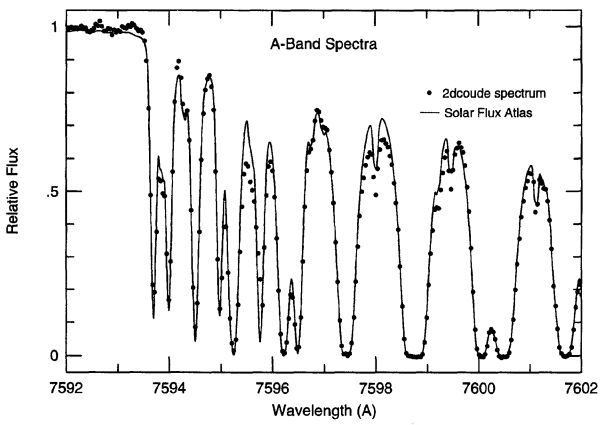

FIG. 11—Part of the telluric A-band O_2 spectrum. The 2dcoudé spectrum is of integrated sunlight, from the solar port; it is compared to the Kurucz et al. (1984) solar-flux atlas.

individual (dark-subtracted) laser observation frames, using the IRAF data reduction utilities. Then, because the laser line did not fall exactly parallel to a CCD column, we extracted individual spectrum strips of 10 pixels in height. These spectra then were linearly interpolated and shifted in wavelength before co-addition to achieve the final spectrum. The linear interpolation in wavelength was necessary to avoid introduction of false features in the spectra (the slope of the laser profile changes sharply at several points). The inevitable price paid was a small loss of effective resolution: a blunting of the peak intensity and an increase of profile breadth. The original resolving power was estimated from the individual extracted strips before shifting: the FWHM in the individual strips was 1.57 ± 0.05 pixels, each pixel being 0.01524 mm. At the known reciprocal dispersion of 2.234 Å mm^{-1} this is equivalent to 0.053 Å, yielding a resolution $R=120{,}000$.

The resolution was degraded to about 1.70 pixels FWHM due to interpolation effects in the shift-and-add method. The profile is undersampled with the TI CCD, using the narrow slit with which these observations were obtained. An accurate estimate of the intensity of the peak is lost due to the finite width of the pixel; thus the true limiting optical resolving power is actually somewhat higher than 120,000. It should be noted that the resolving power goal for this camera, using 24 μm pixels, was $R=60{,}000$.

It is clear from Fig. 10 that the echelle grating E2 is an exceptionally clean ruling totally free from Rowland ghosts within the 12 Å region observed, to a limit 10^{-5} of the parent line, where the detection limit is set by the noise in the far wings. There is an asymmetry on the red wing extending out 1 Å which may be due to charge transfer inefficiency in the TI CCD; its intensity is less than 10^{-3} of the peak. A shoulder on the blue wing 10^{-4} below the peak may be a residual satellite laser line; this extends out about 1 Å. For this profile the FWHM is 0.057 Å, the full width at 1/10 peak is 0.118 Å, and the full width at 1/100 peak is 0.192 Å. At 1/1000 peak the width is still only 0.7 Å. A comparison with published instrumental profiles for other spectrographs shows this to be excellent, yet Griffin's cautions regarding spectrophotometry still hold due to the extended wings.

5.2 Scattered Light

An additional direct measure of the scattered light in 2dcoudé was obtained from a solar spectrum in the region of the telluric A band, using sunlight diffused onto the spectrometer slit from the "solar port" in the roof of the coudé slit room. The A-band O_2 lines are extremely deep, absorbing essentially all the solar flux at the line centers. The detector was the TI CCD. The spectrum was reduced to final form in the usual way except that no flat-field lamp division was performed. In Fig. 11 we compare the reduced 2dcoudé spectrum to that of the higher-resolution solar-flux atlas by Kurucz et al. (1984). The solar-flux atlas was smoothed approximately to the resolution of the 2dcoudé data via simple running means of the atlas data. The deepest parts of the A-band features are virtually indistinguishable between these spectra, showing that scattered light was not a serious problem for 2dcoudé at the wavelengths of the O_2 A band, even before installation of the straylight mask described in Sec. *4.6.5.*

5.3 Stellar Spectra

The 2dcoudé echelle spectrometer has been scheduled for general observer use since 1992 April. Most observations to date have been made with a TI 800×800 CCD. A Tektronix 512×512 CCD and a borrowed Tektronix 2048×2048 with 21 μm pixels have been used for a few nights. We tested the photometric accuracy of the spectrometer with the TI chip by observing stars with published equivalent width measurements. In Fig. 12 we show a small section of the spectrum of Arcturus; this spectrum was obtained with the spectrometer entrance slit matched to two TI 15 μm pixels, for an effective resolving power $R\simeq95{,}000$. This spectrum, when compared to a similar section of the Arcturus Atlas (Griffin 1968), shows that the absorption lines have been resolved. Essentially all features are real in our spectrum. The higher resolution of the Arcturus Atlas produces slightly deeper ab-

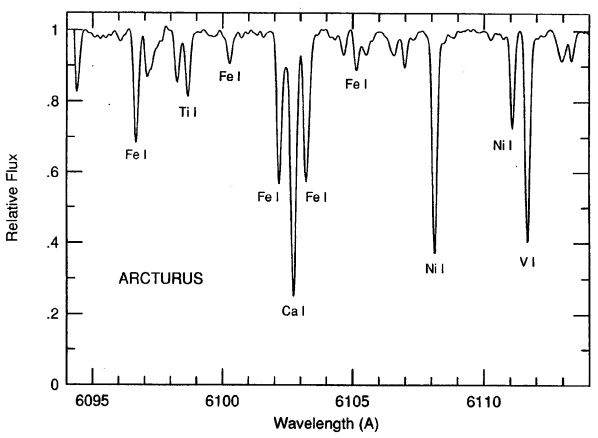

FIG. 12—Part of the 2dcoudé spectrum of Arcturus. This spectral region has been chosen for display because it is a relatively uncrowded one and because it has no strong telluric water-vapor absorption features.

sorption features than seen in Fig. 12, while the higher S/N of our spectrum, a result of the use of a low-noise CCD detector, reveals more faint absorption lines.

In Fig. 13 we compare published equivalent widths for two stars with those measured on our spectra. For Arcturus the literature values are from Mäckle et al. (1975), and for HD 122563, a much-studied very metal-poor giant, the literature values are from Sneden and Parthasarathy (1983). The 2dcoudé CCD images were reduced to one-dimensional spectra using both standard IRAF routines and special software written by James McCarthy and Austin Tomaney for echelle spectrum reductions (these routines, which employ improved techniques for scattered light subtraction and flat-field image division, have been adapted to the IRAF operating environment). Equivalent width measurements were accomplished with an interactive software package (Fitzpatrick and Sneden 1987) designed to work with high-resolution spectra. Gaussian profiles were used to approximate the absorption line shapes.

The 2dcoudé equivalent width scales agree fairly well with those in the literature. For Arcturus, the mean difference, in the sense EW (2dcoudé) *minus* EW (Mäckle et al.), is 4.7±0.8 mÅ for 45 lines (with the standard deviation of a single measurement σ=5.5 mÅ). For HD 122563, the mean difference EW (2dcoudé) *minus* EW(Sneden and Parthasarathy) is −1.6±1.1 mÅ, for 29 lines (σ=5.9 mÅ). We expect the 2dcoudé equivalent widths for HD 122563 to be superior to those of Sneden and Parthasarathy, for their data were obtained at much lower resolution with an intensified Digicon silicon diode array. The mean difference in equivalent widths with the Mäckle et al. data is somewhat larger than hoped for, but may be due to continuum placement and line profile approximation differences, which are difficult to quantify here. An investigation of the causes of this small offset in equivalent width scales is beyond the scope of this paper, but should be pursued with a larger data set in the future.

5.4 Efficiency and Limiting Magnitude

On 1993 June 10 UT a thinned Tektronix 512×512 CCD with 27 μm pixels and otherwise similar to the Tektronix 2048×2048 was used in observations designed to estimate the magnitude limit of the 2dcoudé. One-hour observations centered at 5500 Å were obtained on four solar-type stars in the range $8.3<V<10.7$ at air mass 1.06 to 1.85. The slit width was 1.20 arcsec and the seeing was reported as not much better than 2 arcsec FWHM, but improving (as judged by the width of the spectral orders at the CCD, perpendicular to dispersion). The resolution limited by the pixel width was R=56,000. The calculations included adjustments to simulate resolving power R=60,000 and the upper envelope of a plot of observed minus cataloged magnitudes $m_o - V$ was extrapolated to airmass 1.0, using the monochromatic 5500-Å extinction coefficient 0.19 magnitudes/airmass given by Allen (1963). The resulting limit, referred to an observation at the zenith, is V=11.2 for S/N =100 at R=60,000 at 5500 Å in a 1-hr exposure.

A star of magnitude V=11.2 with one airmass of extinction will deliver 1.24×10^3 photons/Å s^{-1} to the telescope at 5500 Å over the obscured area of the objective mirror. At resolving power R=60,000 with two reduced pixels (co-added across the width of the spectrum) per resolution FWHM each pixel will receive 2.04×10^5 photons/hr in a

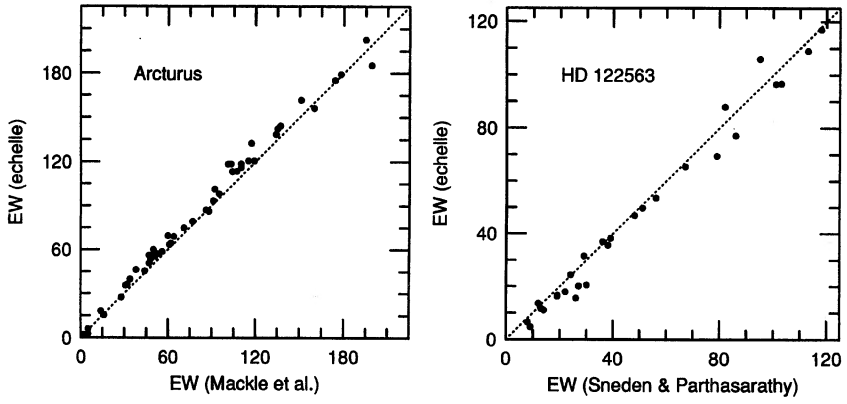

FIG. 13—Comparisons of 2dcoudé and literature equivalent widths (in units of mÅ) for two bright stars.

lossless system. In a spectrum with S/N=100, neglecting sky and detector noise, only 10^4 photons/(reduced pixel) are actually detected, hence the total throughput efficiency was 4.9% under the test conditions. From the relationships given by Diego (1985) we can apply a slit correction: for 2″–2.″5 seeing and a 1.″2 slitwidth, 8″ slit length, the slit transmission is 30%–42%. The system efficiency with no slit is therefore 12%–16%, including telescope, spectrometer optics, and detector quantum efficiency.

We can also predict the expected efficiency of the telescope and 2dcoudé using the combined losses of individual components throughout the system. The primary, secondary, and tertiary mirrors of the 2.7-m telescope and one spectrograph mirror are aluminized. All other mirrors have overcoated silver surfaces,[7] and all refractive elements are A-R coated with average loss 0.5% per surface. Internal transmittance losses of the fused silica corrector plates and prisms are negligible. Assuming reflectances similar to those measured some years ago for the mirrors of the telescope and coudé spectrograph, averaging 88% at 6600 Å for aluminum and 97.5% for silver, and using the known 22% obscuration of the primary mirror by the coudé secondary support the telescope optical efficiency is 50% and that of the spectrometer is 47%, excluding slit losses and CCD quantum efficiency. The Milton Roy certificate for Echelle E2 gave its efficiency as 67% at the blaze maximum in order 63 when purchased. It has 7% vignetting loss when centered on the blaze. The CCD RQE at 5500 Å is about 77% and it is behind an uncoated silica window (93%); the overall throughput efficiency is thus predicted to be about 16% at the blaze peak nearest the photometric V band. Thus the predicted and measured efficiency of the full system, telescope plus spectrometer plus detector, are in agreement and we can accept a figure of approximately 15% in the V band for the slitless throughput efficiency of the full system including detector.

6. CONCLUSION

We have described a new cross-dispersed high-resolution broadband spectrometer giving resolving power up to 250,000. A unique aspect of the optical design is the variation on a white-pupil spectrograph principle. This spectrometer is now in operation at the 2.7-m telescope at McDonald Observatory. Tests of its slit resolution profile, "speed" and photometric accuracy show that the spectrometer is performing at or exceeding its design parameters.

Design and construction of 2dcoudé were supported by the National Science Foundation, through Grant No. AST 8716024. We are grateful for further financial support from NASA (for funding the new echelle grating) and from the University of Texas at Austin (through the College of Natural Sciences grant matching fund program). We thank Harland Epps for useful suggestions in the optical design, John Good for engineering design and Renée Beveridge for reduction and analysis of some of the stellar images. David Doss obtained the images of the laser spectrum. Genesee Optical Software, Inc., and Autodesk, Inc., provided copies of GENII-PC and AUTOCAD releases 10 and 11 at generous educational discounts.

[7]FSS-99, Denton Vacuum, Inc., Cherry Hill Industrial Center, 2 Pin Oak Lane, Cherry Hill, NJ 08003.

TABLE 1
Refractive Indices

Wavelength (Å)	Cargille 50350 n	Fused Silica n	Computed Interface Reflectance	% Transmittance 1 cm path, Oil
3370	1.485	1.479211	3.8×10^{-6}	99
4047	1.4727	1.469607	1.1×10^{-6}	99
4861	1.4645	1.463129	2.2×10^{-7}	100
4880	1.4643	1.463015	1.9×10^{-7}	100
5461	1.4607	1.460081	4.5×10^{-8}	100
5682	1.4596	1.459182	2.1×10^{-8}	100
5893	1.4587	1.458408	1.0×10^{-8}	100
6328	1.4571	1.457024	7×10^{-10}	100
6563	1.4564	1.456372	9×10^{-11}	100
6943	1.4553	1.455429	2.0×10^{-9}	100
8400	1.4526	1.452658	4.0×10^{-10}	100
10648	1.450	1.449625	1.7×10^{-8}	96
11000	1.450	1.449209	7.4×10^{-8}	99

APPENDIX A: OPTICAL CHARACTERISTICS OF CARGILLE 50350 INDEX MATCHING OIL

Table 1 presents the refractive indices of Cargille oil (Col. 2) and of fused silica (Col. 3). The reflectance of a surface separating media of refractive indices n_1, n_2 (Col. 4) is given by

$$R=\left(\frac{n_2-n_1}{n_2+n_1}\right)^2,$$

while Col. 5 gives the transmittance of Cargille oil. In the thickness used (a few wavelengths of visible light) absorption in the oil is negligible.

The data of Col.'s 2 and 5 are from R. P. Cargille Laboratories data sheet RI-FS-765 dated April 18, 1988; Col. 3 is computed from the Cauchy equation with coefficients supplied by Harland Epps (Lick Observatory).

REFERENCES

Allen, C. W. 1963, Astrophysical Quantities, 2nd ed. (University of London, Athlone), p. 122
Baranne, A. 1972, in ESO/CERN Conference on Auxiliary Instrumentation for Large Telescopes, ed. S. Laustsen and A. Reiz (Geneva), p. 227
Barden, S. C., Armandroff, T., Massey, P., Groves, L., Rudeen, A. C., Vaughnn, D., and Muller, G. 1993, in Fiber Optics in Astronomy II, ASP Conf. Ser., 37, 185
Bloom, A L. 1966, Appl. Opt., 5, 1500
Cottrell, P. L., and Sneden, C. 1986, A&A, 161, 314
Crane, P., Lambert, D. L., and Sheffer, Y. 1994, ApJS (to be published)
Dekker, H., Delabre, B., and D'Odorico, S. 1986, in Instrumentation in Astronomy VI, SPIE 627, 339
Diego, F. 1985, PASP, 97, 1209
Fitzpatrick, M. J., and Sneden, C. 1987, BAAS, 19, 1129
Gies, D. R., and Kullavanijaya, A. 1987, BAAS, 19, 1051
Griffin, R. F. 1968, A Photometric Atlas of the Spectrum of Arcturus (Cambridge, Cambridge Philos. Soc.)
Griffin, R. F. 1969, MNRAS, 143, 319
Harrison, G. R. 1949, JOSA, 39, 522

Hobbs, L. M., and Welty, D. E. 1991, ApJ, 368, 426
Kurucz, R. L., Furenlid, I., Brault, J., and Testerman, L. 1984, Solar Flux Atlas from 296 to 1300 nm (Cambridge, Harvard University)
Lambert D. L., Sheffer, Y., and Crane, P. 1990, ApJ, 359, L19
Loewen, E. G. 1993, Progress Report, NSF Grant AST90-08025, p. 5
Mäckle, R., Griffin, R., Griffin, R., and Holweger, H. 1975, A&AS, 38, 239
MacQueen, P. J., and Tull, R. G. 1988, in Instrumentation for Ground-Based Optical Astronomy Present and Future, ed. L. B. Robinson (New York, Springer), p. 52
Schroeder, D. J. 1987, Astronomical Optics (New York, Academic), pp. 250–251
Schroeder, D. J., and Hilliard, R. L. 1980, Appl. Opt., 19, 2833
Shetrone, M. D., Sneden, C., and Pilachowski, C. A. 1993, PASP, 105, 337
Sneden, C., and Parthasarathy, M. 1983, ApJ, 267, 757
Tull, R. G. 1969, Sky and Tel., 38, 156
Tull, R. G. 1972, in ESO/CERN Conference on Auxiliary Instrumentation for Large Telescopes, ed. S. Laustsen and A. Reiz (Geneva), p. 259
Tull, R. G., Choisser, J. P., and Snow, E. H. 1975, Appl. Opt., 14, 1182
Tull, R. G., and MacQueen, P. J. 1988, ESO Conference on Very Large Telescopes and their Instrumentation, ed. M.-H. Ulrich (Garching), p. 1235
Tull, R. G., Vogt, S. S., and Kelton, P. 1978, Appl. Opt., 17, 574